phys. stat. sol. (a) **205**, No. 6, 1386–1390 (2008) / **DOI** 10.1002/pssa.200778163

physica status solidi a
www.pss-a.com
applications and materials science

Unifying catalyst size dependencies in floating catalyst and supported catalyst carbon nanotube synthesis

M. H. Rümmeli[*,1], F. Schäffel[1], M. Löffler[1], C. Kramberger[1], D. Adebimpe[2], T. Gemming[1], P. Ayala[3], B. Rellinghaus[1], L. Schultz[1], B. Büchner[1], and T. Pichler[1]

[1] IFW Dresden, P.O. Box 270116, 01171 Dresden, Germany
[2] Polymath Interscience, LLC, Ironstone Court, Annapolis, MD 21403, USA
[3] Laboratory of Physics and Center for New Materials, Helsinki University of Technology, P.O. Box 5100, 02150 Espoo, Finland

Received 8 October 2007, revised 19 February 2008, accepted 22 February 2008
Published online 15 May 2008

PACS 61.46.Fg, 68.37.Lp, 81.07.De, 81.15.Fg, 81.15.Gh, 82.33.Ya

[*] Corresponding author: e-mail m.ruemmeli@ifw-dresden.de

Detailed studies with floating catalyst systems, namely, laser evaporation and laser assisted chemical vapour deposition (CVD), enabled the development of a catalyst volume to surface area model which dictates if a single walled carbon nanotube (SWCNT) can emerge or not. The model predicts differences in the case of supported catalysts. It predicts multi-walled carbon nanotubes (MWCNT) will also emerge. This difference arises due to the catalyst/support interaction. Further, the model says that for supported catalysts the catalyst volume to surface area ratio also regulates the tube diameter and the number of walls the nanotube will have. In this contribution, experimental CVD data using predefined catalyst particles on a support are presented and compared with floating catalyst data. The findings for supported catalysts are in full agreement with those predicted by the catalyst surface area to volume model. The data show unified catalyst size dependencies for floating catalyst and supported catalyst carbon nanotube synthesis routes.

1 Introduction To take advantage of the exceptional mechanical [1], electronic [2], and thermal [3] properties of carbon nanotubes (CNT) a key prerequisite is that they be manufactured with greater control than current manufacturing techniques afford. CNT can be synthesised using various methods including arc discharge [4], laser evaporation [5, 6], catalytic pyrolysis of hydrocarbons [7] and plasma-enhanced [8], laser assisted [9] or thermally activated chemical vapour deposition (CVD) [10]. On the whole, carbon nanotubes (CNT) require growth to stem from a catalyst particle. There are, though, instances in which multi-walled carbon nanotubes (MWCNT), as opposed to single-walled carbon nanotubes (SWCNT), have been synthesized without catalyst particles [11, 12]. Successful catalyst particles generally are Ni, Co, or Fe based, however, more recent studies show other metals such as In, Cu, Mg, Ag and Au can also be used for SWCNT formation [6, 14, 15]. Since SWCNT nucleation appears to always require a catalyst particle and MWCNT is most successfully achieved through catalyst particles, a great deal of attention has been paid to the catalysts role in forming the embryonic stage of CNT. However, their full role has yet to be determined. This is in part due to conflicting results, which may indicate that several mechanisms exist. This is highlighted, for example, by different studies in chemical vapour deposition (CVD) based synthesis routes in which the catalyst resides on a substrate, henceforth referred to as substrate-based CVD. Some substrate-based CVD studies suggest that the catalyst is not in a liquid state at nucleation and it is argued that the initial embryonic cap of a SWCNT forms via surface diffusion of C [16]. On the other hand, other substrate-based CVD studies point to the diameter of the catalyst particle actually templating the diameter of the obtained CNT [17, 18], and it is argued that the catalyst particles are in a liquid state allowing bulk diffusion of C [19]. In this contribution we present detailed studies from two floating catalyst techniques, namely, laser evaporation and laser assisted CVD, along with supported

catalyst CVD studies. The results point to common catalyst size dependencies in that the catalyst volume to surface area ratio defines the type of nanostructure to emerge. With floating catalysts this catalyst volume to surface area ratio dictates if a SWCNT can grow or not. In the case of supported catalysts the catalyst volume to surface area ratio regulates the CNT diameter and the number of walls the CNT will have. The results further our understanding of CNT growth processes.

2 Experimental The pulsed laser evaporation setup and description can be found elsewhere [20]. In brief, an alumina tube (outer diameter = 80 mm) with an inner alumina tube (outer diameter = 25 mm) sit in a horizontal oven. At one end a removable cold finger with a target holder and target placed at the end sits within the inner alumina tube. At the other end are a gas entry port and a window for coupling the pulsed laser beam (10 Hz, 1064 nm). Two sets of SWCNT using the following catalyst mixes were explored, Pt/Rh/Re (18.98 : 3.22 : 0.8 wt%) and Ni/Co (10 : 10 wt%). These particular catalyst mixes were chosen for high yield SWCNT production and also for their different synthesis temperature windows. In the case of Pt/Rh/Re, the catalyst mix also yields magnetically pure SWCNT [20]. These catalyst mixes are mixed with research grade graphite and are pressed into circular targets (13 mm diameter) for mounting onto the target holder. In all cases the purities of the materials, including the graphite were >99.9%. Various buffer gases (Ar, Xe, Kr, He, Ne and N_2) were explored. All gases were of research grade.

For the laser assisted CVD studies, a similar setup as for the laser evaporation was used [21]. In this case the targets are of a pure metal mix of Ni, Co and Mo (50 : 40 : 10 wt%). In addition, no buffer gas was used, instead a hydrocarbon is used which serves as the carbon feedstock. The hydrocarbons investigated were ethanol (50 mbar) and methane (1 bar).

For the CVD studies, iron nanoparticles were deposited on thermally oxidised silicon with an additional 10 nm alumina layer using an inert gas condensation method based on a direct current sputtering process [22]. Witness plates were obtained during the procedure for pre-CVD analysis of the particles. The CVD reactions were conducted at 800 °C with cyclohexane (60 mbar) as the carbon feedstock. Details of the CVD reaction are given in Ref. [22].

The products from the laser evaporation and CVD routes were analysed using transmission electron microscopy (TEM) – (FEI Tecnai F30, 300 kV), Fourier transform Raman spectroscopy (Bruker IFS100) and Fourier transform optical absorption spectroscopy (OAS) – (Bruker IFS113V/88) in the energy range 0.35 eV to 2.35 eV. Details on the preparation of the TEM grids and OAS films can be found elsewhere [6].

The sample yields (SWCNT/amorphous species) were determined by optical absorption techniques, viz. the relative purity is determined from the intensity of the first semiconducting peak of the SWCNT to the background intensity. This is because the OAS spectrum reflects the difference in electronic states from SWCNT and amorphous carbon.

3 Results and discussion In our systematic laser evaporation studies we explored various parameters, namely, gas type (He, Ne, Ar, N_2, Kr and Xe), catalyst concentration and type and temperature (800 °C to 1600 °C). The effect of these parameters on the mean diameter and diameter distribution as well as yield was determined primarily using OAS. OAS has been shown to be a powerful tool for such studies via the SWCNT absorption peaks arising from transitions between van Hove singularities. The studies on the role of gas type showed that as the oven temperature was raised, the mean diameter increased in a linear manner until at the higher temperatures the mean diameter increase levels off to a constant value [14, 23]. This upper levelling off of the mean diameter with temperature increase we term the upper saturation diameter. Regards the linear change in mean diameter of the SWCNT with oven temperature, the rate of change in diameter varied between the gases such that the gradient became less steep as the gas thermal conductivity decreased.

The upper saturation diameter remained the same for all gases with the exception of He. He has a significantly higher thermal conductivity relative to the other investigated gases. In this case the saturation diameter was lowered. At yet lower oven temperatures the diameter dependence also saturates to a constant level. This lower mean diameter limit we call the lower saturation diameter. Figure 1(i) shows the diameter dependence with temperature including the upper and lower saturation temperature. The laser assisted CVD studies showed a similar dependence of the mean diameter of the obtained SWCNT on temperature, showing a lower diameter saturation at low temperatures and then a linear increase in mean diameter. In laser assisted CVD the upper temperature attainable is limited since at temperatures above ca. 900 °C hydrocarbons tend to self-pyrolise, self-polymerise and condense to light and heavy oils [24, 25]. This leads to undesirable samples. Hence we were unable to explore temperatures above 1000 °C with laser assisted CVD.

In terms of the yield (SWCNT to amorphous species), in laser evaporation, N_2 provided the highest yields and He

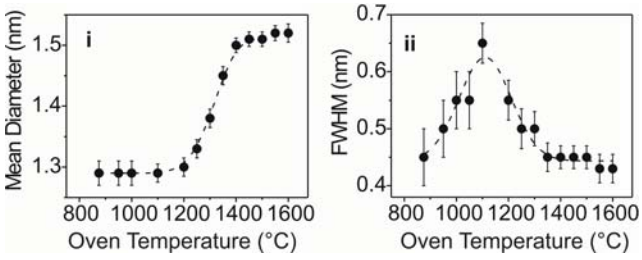

Figure 1 Mean diameter and diameter distribution dependencies in laser evaporation (catalyst: Pt/Rh/Re mix, gas: N_2). (i) SWCNT mean diameter variation with oven temperature. (ii) Diameter distribution FWHM versus oven temperature.

led to the lowest yields. The yield was also found to be dependent on the catalyst content in the ablation target. As the catalyst content increases so does the yield up to a catalyst content of ca. 10 at%. Increasing the catalyst content above 10 at% leads to a rapid drop in yield. However, regardless of the changes in yield, *no* changes in the diameter dependence with catalyst concentration were observed. Slight differences in the upper and lower saturation diameters are observed for different catalyst types. With regards the yield dependencies of laser assisted CVD the yield was found to be feedstock dependent. Better yields were obtained with ethanol as the feedstock as opposed to methane. As with laser evaporation the yield is dependent on the temperature also rising to a maximum and then decreasing.

We also explored the variation of the full width at half maximum (FWHM) of the diameter distribution with respect to oven temperature for both the laser evaporated and laser assisted CVD samples. This dependence for the laser-evaporated sample is illustrated in Fig. 1(ii). It shows the FWHM increasing to a maximum after which it declines. In the case of the laser assisted CVD data [21] the FWHM of the diameter distribution increases with temperature. Due to the limited temperatures we could use we could not ascertain if the increasing FWHM reached a maximum. Further the FWHM were about 2 times larger than found with the laser evaporated samples at similar temperatures.

The laser assisted CVD route also allowed us to explore the role of carbon feed-rate via the feedstock pressure or flow. The data showed that increasing the pressure decreases the mean diameter. This diminishes the yield also. An increasing flow rate increases the the relative mean diameter up to a steady value (saturation). The yield runs through a maximum just before the mean diameter starts to saturate.

We now bring together the various experimental observations on the diameter and yield dependencies with floating catalysts in a detailed microscopic catalyst volume to surface area model. This is then applied to substrate based CVD data. The above-discussed behaviours can be explained in a model where a nucleation window exists [23]. This window depends on the catalyst volume to surface area (V_c/A_c) and second window in which the carbon saturated catalyst particles precipitate their carbon. This second *precipitation* window is dependent on various factors such as the catalyst-carbon eutectic point and the catalyst carbon absorption coefficient. The key aspect of this model, as applied to floating catalysts, is that SWCNT are only formed when the nucleation and precipitation windows overlap [23]. Figure 2 illustrates the model and shows the requirement of the SWCNT formation window where only catalyst particles, which precipitate sufficient carbon to form a hemisphere, nucleate SWCNT. Catalyst particles that are too small cannot form a stable cap for nucleation and particles, which are too big also do not nucleate SWCNT since they are simply encapsulated by the precipitating carbon. Thus, it is also clear that as one changes the amount of carbon dissolved into a molten particle one

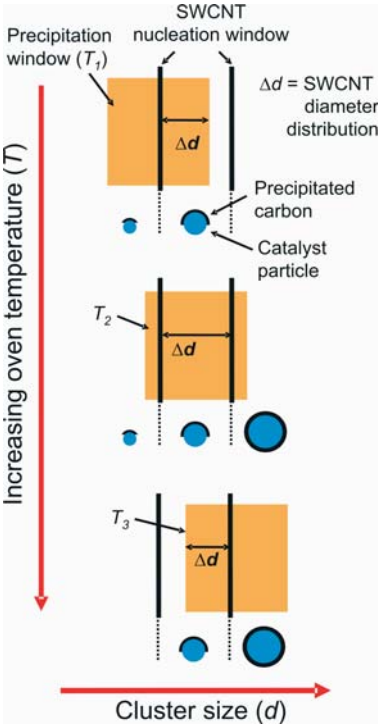

Figure 2 (online colour at: www.pss-a.com) Proposed nucleation mechanism. The schematic shows the precipitating particle diameter distributions at three snapshots in time for 3 increased oven temperatures ($T_1 < T_2 < T_3$). Inside the SWCNT formation window stable nucleation caps allow SWCNT growth. SWCNT are only formed in the overlap between the precipitating catalyst (size) distribution and SWCNT growth window. The amount of overlap determines the SWCNT diameter distribution (Δd) and mean diameter. Particles that are too big are encapsulated by graphite and particles that are too small are unlikely to form a stable cap.

can control the precipitating cap at nucleation. This we observe as a reduction in the mean diameter when increasing the feedstock pressure in the laser assisted CVD reaction. Increasing the pressure is equivalent to increasing the carbon feed-rate into the catalyst particle, which will further increase the likelihood of encapsulation. The carbon feed-rate into the catalyst particle is also catalyst size dependent. Since the incorporation rate is surface area dependent and the total absorption of carbon is volume dependent, the relative dependence of the incorporation rate is lessened as the catalyst particle size increases.

However, the overall effect of increasing the pressure is a more rapid particle encapsulation at nucleation. Thus, the formation of appropriate hemispherical caps for nucleating SWCNT occurs for smaller particles, viz. a reduction in the mean diameter of the obtained SWCNT. Thus, there are competing processes between the catalyst size, carbon feed-rate and precipitation-rate. The exact contribution from each will be dependent on various factors such as the temperature difference, pressure, catalyst choice and laser power. The diameter dependence on the feedstock flow

rate follows a similar argumentation. Low gas velocities mean that the residence time of the catalyst particles in the active zone is lengthened. This leads to a higher carbon/metal ratio due to more time being available for precursor decomposition. This results in CNT with smaller diameters. In turn the mean diameter increases with increasing gas flow.

The model described here and in [23] predicts that the catalyst volume to surface area (V_c/A_c) dependencies for supported catalysts in CVD growth will be different than for floating catalysts. It predicts that since the catalyst resides on the support the catalyst/support interaction will prevent precipitating carbon from encapsulating the particle. Instead, once a hemispherical carbon cap has formed, since encapsulation is prevented by the presence of the support, a second hemispherical cap begins to form underneath the first cap. Further excess carbon will form new hemispherical caps each within the previously formed cap. In other words, as the catalyst particle size increases one goes from SWCNT formation to double walled carbon nanotubes (DWCNT) to higher order MWCNT. This process is illustrated in Fig. 3. Figure 3 also highlights the difference for the floating catalyst scenario where excess carbon leads to particle encapsulation.

The model also states that the outer diameter of a CNT from supported catalyst CVD should be defined by the first precipitating cap (outer CNT wall). To verify the model as applied to supported catalysts we conducted studies in which we deposit predefined (size and density) catalyst particles onto substrates in a controlled manner. This enabled us to directly examine the catalyst particles *prior* to CVD synthesis and to compare them with the resultant CNT in terms of their diameter and number of walls [18]. This was accomplished by TEM studies in which a statistical analysis of the catalyst particles (pre-reaction), CNT outer diameter and number of walls were conducted. Typically 200 to 400 catalyst particles measured (each two times) and 100 to 200 CNT were investigated (across at least two positions) per sample.

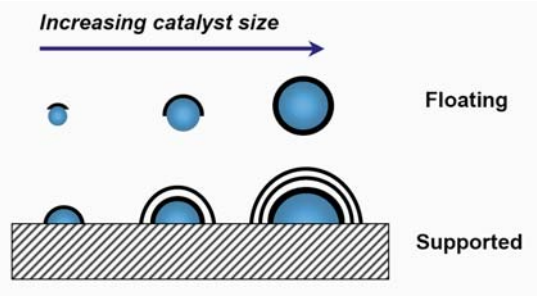

Figure 3 (online colour at: www.pss-a.com) Illustration of the catalyst volume to surface area dependencies between floating catalysts and supported catalysts. With floating catalysts excess carbon at nucleation leads to encapsulation (preventing SWCNT growth) whilst for supported catalysts excess carbon forms new caps within the previous cap since encapsulation is prevented by the catalyst support interaction.

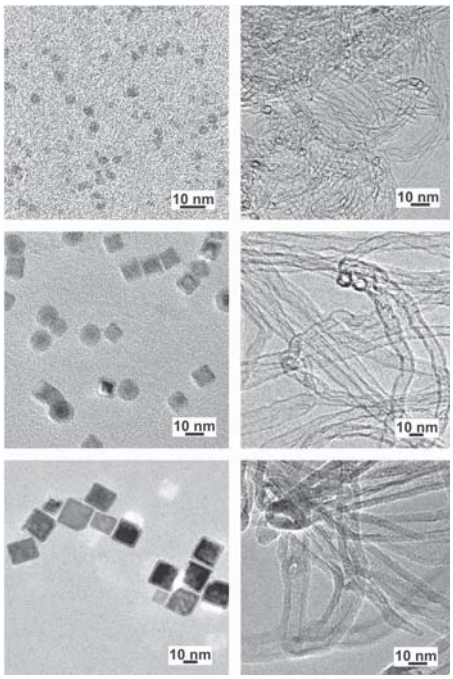

Figure 4 Left panels: TEM images of the starting Fe catalyst particles. Increasing size from top to bottom. Right panels: Resultant CNT after CVD synthesis on $Si/SiO_2/Al_2O_3$.

Figure 4 shows typical TEM images for catalyst (Fe) particles with different size distributions and their resultant CNT after CVD synthesis. From these images one can easily observe the increasing CNT outer diameter and number of walls as the catalyst diameter increases. A detailed statistical analysis provides quantified data on the relationship between the resultant CNT diameter and number of walls with catalyst size. The data is given in Fig. 5(i) and (ii) respectively.

In Fig. 5(i). one sees that within the particle diameter range studied (2 nm to 20 nm) there appears to be a direct relationship between the catalyst diameter and the outer diameter of the resultant CNT. This is in agreement with the model (for supported catalysts), which dictates that the outer diameter of the CNT is templated by the first cap that forms. In addition, the model says that as the catalyst particle increases so does the volume to surface area ratio and hence more excess carbon will be available for the forma-

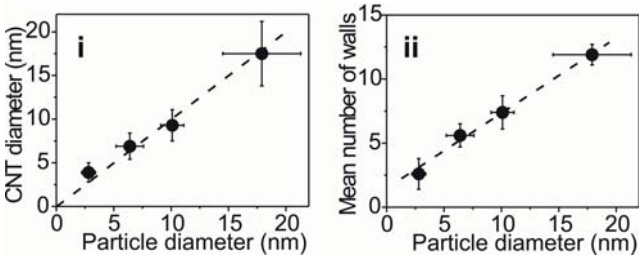

Figure 5 CNT mean diameter (i) and mean number of walls (ii) versus catalyst particle diameter in substrate based CVD. The error bars represent the standard deviation among the data.

tion of further caps within the previously formed cap (see Fig. 3). The number of caps determines the number of walls in the CNT and thus we would expect to see an increase in the number of walls as the catalyst particle diameter increases. Figure 5(ii). shows the number of CNT walls versus the catalyst particle diameter. It clearly shows that the number of walls increases with increasing catalyst diameter in full agreement with the catalyst volume to surface area model described above.

4 Conclusions To conclude, we have conducted studies on the formation of CNT in laser evaporation, laser assisted CVD and substrate based CVD. The floating catalyst data was used to develop a model in which the volume to surface area dictated whether a SWCNT would emerge or not. The catalyst volume to surface area at the point of nucleation explains this. Insufficient carbon at nucleation does not enable a hemispherical cap (for SWCNT growth) to form and too much carbon simply leads to the catalyst being encapsulated. Only when a stable hemispherical cap forms does SWCNT growth occur. The model as applied to supported catalysts predicts that, due to the catalyst support interaction, encapsulation is not possible and this instead leads to multiple caps forming when excess carbon is available. Thus, as the catalyst particle size increases one goes from SWCNT formation to double walled carbon nanotubes (DWCNT) to higher order MWCNT. In this contribution, CVD studies with predefined catalyst particles on supports show this predicted behaviour and lend credence to the catalyst volume to surface area model. The data points to unified catalyst size dependencies in floating catalyst and supported catalyst carbon nanotube synthesis.

Acknowledgements This work is financially supported by the DFG (PI 440/4). FS acknowledges funding from the Cusanuswerk. CK thanks the International Max Planck Research School "Dynamical Processes in Atoms, Molecules and Solids".

References

[1] M. M. Treacy, T. W. Ebbesen, and J. M. Gibson, Nature **381**, 678 (1996).
[2] H. J. Dai, E. W. Wong, and C. M. Lieber, Science **272**, 523 (1996).
[3] J. Hone, M. Whitney, C. Piskoti, and A. Zettl, Phys. Rev. B **59**, R2514 (1999).
[4] S. Iijima, Nature **354**, 56 (1991).
[5] T. Guo, P. Nikolaev, A. Thess, D. T. Colbert, and R. E. Smalley, Chem. Phys. Lett. **243**, 49 (1995).
[6] M. H. Rümmeli, E. Borowiak-Palen, T. Gemming, T. Pichler, M. Knupfer, M. Kalbác, L. Dunsch, O. Jost, S. R. P. Silva, W. Pompe, and B. Büchner, Nano Lett. **5**, 1209 (2005).
[7] M. Endo, K. Takeuchi, K. Kobori, K. Takahashi, H. W. Kroto, and A. Sarkar, Carbon **33**, 873 (1995).
[8] Z. F. Ren, Z. P. Huang, J. W. Xu, J. H. Wang, P. Bush, M. P. Siegal, and P. N. Provencio, Science **282**, 1105 (1995).
[9] M. H. Rümmeli, C. Kramberger, M. Löffler, M. Kalbác, H.-W. Hübers, A. Grüneis, A. Barreiro, D. Grimm, P. Ayala, T. Gemming, F. Schäffel, L. Dunsch, B. Büchner, and T. Pichler, Nanotechnology **17**, 5469 (1996).
[10] W. Z. Li, S. S. Xie, L. X. Qian, B. H. Chang, B. S. Zou, W. Y. Zhou, R. A. Zhao, and G. Wang, Science **274**, 1701 (1996).
[11] J. J. Schneider, N. I. Maksimova, J. Engstler, R. Joshi, R. Schierholz, and R. Feile, Inorg. Chim. Acta, DOI: 10.1016/j.ica.2006.10.025 (2006).
[12] W. Merchan-Merchan, A. Savaliev, L. A. Kennedy, and A. Fridman, Chem. Phys. Lett. **354**, 20 (2002).
[13] E. J. Bae, W. B. Choi, K. S. Jeong, J. U. Chu, G.-S. Park, S. Song, and Y. U. Yoo, Adv. Mater. **14**, 277 (2002).
[14] M. H. Rümmeli, A. Grüneis, M. Löffler, M. Jost, R. Schönfelder, C. Kramberger, D. Grimm, T. Gemming, A. Barreiro, E. Borowiak-Palen, M. Kalbác, P. Ayala, H.-W. Hübers, B. Büchner, and T. Pichler, phys. stat. sol. (b) **243**, 3101 (2006).
[15] D. Takagi, Y. Homma, H. Hibino, S. Suzuki, and Y. Kobayashi, Nano Lett. **6**, 2642 (2006).
[16] S. Hofmann, C. Ducati, J. Robertson, and B. Kleinsorge, Appl. Phys. Lett. **83**, 135 (2003).
[17] Y. Zhang, Y. Li, W. Kim, and H. Dai, Appl. Phys. A **74**, 325 (2002).
[18] F. Schäffel, C. Kramberger, M. H. Rümmeli, D. Grimm, E. Mohn, T. Gemming, T. Pichler, B. Rellinghaus, B. Büchner, and L. Schultz, Chem. Mater. **19**, 5006 (2007).
[19] J. A. Rodriguez-Manzo, M. Terrones, H. Terrones, H. W. Kroto, L. Sun, and F. Banhart, Nature Nanotechnol. **2**, 307 (2007).
[20] M. H. Rümmeli, M. Löffler, C. Kramberger, F. Simon, F. Fülöp, O. Jost, R. Schönfelder, A. Grüneis, T. Gemming, W. Pompe, B. Büchner, and T. Pichler, J. Phys. Chem. C **111**, 4094 (2007).
[21] M. Löffler, M. H. Rümmeli, C. Kramberger, E. Borowiak-Palen, R. Klingeler, T. Gemming, B. Büchner, and T. Pichler, Chem. Mater. **20**, 128 (2008).
[22] F. Schäffel, C. Kramberger, M. H. Rümmeli, R. Kaltofen, D. Grimm, A. Grüneis, E. Mohn, T. Gemming, T. Pichler, B. Büchner, B. Rellinghaus, and L. Schultz, phys. stat. sol. (a) **204**, 1786 (2007).
[23] M. H. Rümmeli, C. Kramberger, M. Löffler, O. Jost, M. Bystrzejewski, A. Grüneis, T. Gemming, W. Pompe, B. Büchner, and T. Pichler, J. Phys. Chem. B **111**, 8234 (2007).
[24] C. Descamps, L. Vignoles, O. Féron, F. Langlais, and J. Lavenac, J. Electrochem. Soc. **148**, 695 (2001).
[25] R. P. Rodgers, P. T. A. Reilly, W. B. Whitten, and J. M. Ramsey, Carbon **41**, 1469 (2003).

